Proceedings of ASME Turbo Expo 2011
GT2011
June 6-10, 2011, Vancouver, British Columbia, Canada

GT2011-46018

HYDRODYNAMIC ANALYSIS OF COMPLIANT FOIL BEARINGS WITH MODIFIED TOP FOIL MODEL

Fangcheng Xu, Zhansheng Liu, Guanghui Zhang, Liang Xie
School of Energy Science and Engineering
Harbin Institute of Technology
Harbin, Heilongjiang, China

ABSTRACT

The mathematical model of film thickness is developed with considering the compressibility of the gas and the deformation of the foil in this paper. By employing the Newton-Raphson method and the finite difference method, the compressible gas lubricated Reynolds equation and the film thickness equation are solved coupling together. The static characteristics such as pressure distribution and film thickness distribution for equivalent bump foil stiffness model are obtained to verify the validation of the proposed method. The gas film thickness model is modified by modeling the top foil as the one dimension curved beam, to meet the case of the real physical model. The numerical results of this modified structural model are compared with the other finite element top foil models. It indicates that the pressure distribution for bump foil gas bearing is in good agreement with the test data.

INTRODUCTION

Bump-type foil bearings are compliant, self-acting hydro-dynamic air bearings which are used in high-speed rotating machinery such as turbo expander etc [1]. Compared with oil bearings and rolling element bearings, these bearings have excellent reliability, environment durability and can be operated at high speeds and temperatures [2]. Moreover, the foil bearings have less environmental pollution because the lubricate media is gas. The main process of predicting bump-type foil bearings is modeling the foil structure and solving compressible gas lubricated Reynolds equation coupled with the compliant surface.

Blok and van Rossum [3] did analytical work in foil bearing analysis and design in the early 50's, but only in the last two decades the interest in this type of bearing has increased considerably. In 1975 Wallowit and Anno [4] first gave the theoretical model of a single bump static stiffness equation using mechanical beam model. In this bump static stiffness model, the two ends of bump were fixed and the friction between the bump foil and top foil were not considered. This bump static stiffness equation was used by Heshmat et al to analysis gas lubricated foil journal bearing and gas lubricated compliant thrust bearing [5, 6]. Peng and Khonsari [7, 8 and 9] employed this static stiffness equation to predict the hydrodynamic performance of a foil journal bearing such as load-capacity and film thickness. The model was established based on the compliance of the bearing surface. Iordanoff [10] presented a very simple method for an aerodynamic compliant foil thrust bearing. In order to carry out the calculation faster, the structural analysis has been simplified. The model considered the different stiffness of welded bump and free bump, which was different from the models mentioned in the above literatures.

Some other authors established finite element model of bump foil and top foil to predict hydrodynamic performance of foil journal bearings. Le Lez et al. [11] proposed a new bump-type foil bearing structure analytical model which accounted for friction interfaces, bump interactions, and nonisotropic stiffness, then finite element method is used to simulate. The model that described the FB structure as a multidegree of freedom system of interacting bumps. Each bump included three degrees of freedom linked with elementary springs. Lee et al. [12] modeled the top foil as a elastic beam-like to present the effects of bump stiffness on the static and dynamic force performance of gas foil bearings. The bump is represented by a linear spring coefficient. San Andrés and Kim [13] analyzed gas foil bearings integrating finite element top foil models. They used more complex finite element (FE) models coupled the elastic deformations of the 2D shell and 1D beam-like top foil to the bump deflections as well as to the gas film hydrodynamics. The results of predictions like

journal attitude angle and minimum film thickness were compared with a gas foil bearing experiment data decades ago and illustrated the sagging phenomenon clearly.

Kim et al. [14] used a 1-D analytical beam model of the top foil for prediction of top foil deflection and sagging effects under hybrid (both hydrostatic and hydrodynamic) mode. Furthermore, Kim and Creary [15, 16] designed, manufactured and modeled mesoscale foil bearings for palm-sized turbomachinery. The radius of gas foil bearings mentioned is only several millimeters which is far smaller than traditional gas foil bearings. In this scale, the curvature of top foil may not be neglected when modeling.

In this paper, a mathematical model of film thickness is developed with considering the compressibility of the gas and the deformation of the foil. The Newton-Raphson method and the finite difference method are employed to solve the coupled Reynolds equation and film thickness equation. A top foil model is developed as the one dimension curved beam. The finite element method and the finite difference method are coupled together to predict this foil bearing model. Predictions are compared with other numerical results and experimental results published in the literature.

NOMENCLATURE

$c_{Bi,j}$	Equivalent viscous damping coefficient of bump *Bi*
e	Journal eccentricity (m)
f	Bump friction coefficient
$f_{Bi,j}$	Total pressure force on a bump with index *Bi*
h	Gas film thickness (m)
$h_{\min}$	Minimum gas film thickness (m)
h_B	Bump height (m)
$\bar{h}$	Dimensionless gas film thickness
$k_{Bi,j}$	Stiffness coefficient of bump *Bi*
l	Half of the bump length (m)
l_x	Foil arc circumferential length (m)
m	Element number between two adjacent bumps
p	Gas pressure (Pa)
p_a	Ambient pressure (Pa)
p_A	Average pressure along axial direction (Pa)
$\bar{p}$	Dimensionless gas pressure
$p_1, p_2 \ldots$	Pressures acting on the top foil element nodes (Pa)
$p_{Bi,j}$	Nodal pressures
$q_{Bi,j}(x)$	Unit force distribution function on top foil
r_0	Outer radius of curved beam (m)
r_i	Inner radius of curved beam (m)
r_n	Radius of neutral axis of curved beam (m)
s	Bump pitch (m)
t_B	Bump foil thickness (m)
t_T	Top foil thickness (m)
$u_1, u_2 \ldots$	Displacement of the top foil in *x* direction (circumferential direction) (m)
$u_{\bar{x}_c}, u_{\bar{z}_c}$	Displacement on ends of curved element in $\bar{x}_c, \bar{y}_c$ directions (m)
v	Top foil deflection in *y* direction (m)
$v_{Bi,j}(\zeta)$	Local top foil sagging function
w_d	Top foil transverse deflection (m)
$w_{Bi,j}(\zeta)$	Local top foil deflection
x, y, z	Coordinates for the structural model (m)
x_c, y_c, z_c	Natural (local) curved element coordinates (m)
$\bar{x}, \bar{y}, \bar{z}$	Dimensionless coordinates
$\bar{x}_c, \bar{y}_c, \bar{z}_c$	Generalized element coordinates (m)
A_b	Area of a bump for FEM (m^2)
C	Radial clearance (m)
E	Beam plate elastic modulus (Pa)
EI	Bending stiffness of the top foil segment
E_B	Bump foil Young's modulus (Pa)
E_T	Top foil Young's modulus (Pa), $E_T = E_B \times S_{fc}$
$F_{\bar{x}_c}, F_{\bar{z}_c}$	Forces on ends of curved element in $\bar{x}_c, \bar{y}_c$ directions
I_z	Area moment of inertia about *z* axis for beam (m^4)
K_f	Structure stiffness per unit area (N/ m^3)
K_{ff}	Bump foil stiffness per unit area for a free-free ends bump (N/ m^3)
K_{fw}	Bump foil stiffness per unit area for a fixed-free end bump (N/ m^3)
K_B	Stiffness of single bump (N/m)
K_{FF}	Stiffness for a free-free ends bump (N/m)
K_{FW}	Stiffness for a fixed-free end bump (N/m)
L	Bearing length (m)
L_b	Length of Euler beam (m)
M_a, M_b	Moment on ends of curved element about $\bar{y}_c$ axis
N_B	Number of bumps (-)
R	Shaft radius (m)
R_c	Radius of centroidal line of curved beam (m)
X, Y	Coordinate system for the inertial axes (m)
X_c, Y_c, Y_c	Global curved element coordinates (m)
β	$\psi / 2$ (rad)
γ	Structure loss factor
$\delta_{Bi,j}$	Deflection of bump *Bi*
ζ	Local coordinate that defines local top foil

	sagging term
η	Air viscosity (Pa•s)
θ	Top foil angular coordinate (rad)
θ_a, θ_b	Rotation on ends of curved element about $\bar{y}_c$ axis
ρ_0	Air density (Kg/ m^3)
υ_b	Bump foil Poisson's ratio (-)
φ	Attitude angle (rad)
ϕ_z	Rotation angle about *z* axis
ψ	Angle of curved beam (rad)
ω	Angular speed of shaft (rpm)
Λ_x	Bearing number

Vectors and matrices

$\{\mathbf{F^G}\}$	Forces vector in global coordinate system
k_e	Finite element stiffness matrix of Euler beam
k^i	Curved beam element stiffness matrix in global coordinate system
$\tilde{\mathrm{k}}^i$	Curved beam element stiffness matrix in the local coordinate system
$[\mathbf{K^B}]$	Bump foil stiffness matrix in global coordinate system
$[\mathbf{K^G}]$	Global stiffness matrix of total model
$[\mathbf{K^T}]$	Top foil model stiffness matrix in global coordinate system
$\{\mathbf{U^G}\}$	Displacement vector in global coordinate system
T^i	Transformation matrix for in-plane loading stiffness matrices
Q, S	Coefficient matrices for curved beam element

ANALYSIS

Bump-type foil bearing structure description

The structure of the first generation bump foil bearing is shown in Fig. 1. It consists of a thin top foil bump and a series of corrugated bump strip layer. The leading edges of both bump and top foil are spot welded to the bearing sleeve, the trailing edges of foils are free. The bump foils act as springs. As the shaft rotates, the top foil can be deflected when air pressure forces on its smooth surface.

There should be some assumptions for simplifying the description of complex analysis:

(1) The change of pressure in the direction of air film thickness is not considered.
(2) The velocity of air on bearing sleeve surface is nil, and the velocity on shaft surface is $R\omega$.
(3) The fluid is idea gas.
(4) The fluid is isothermal.

According to above assumptions, the Reynolds equation can be expressed as follows:

$$\frac{\partial}{\partial x}\left(\frac{ph^3}{\eta}\frac{\partial p}{\partial x}\right)+\frac{\partial}{\partial z}\left(\frac{ph^3}{\eta}\frac{\partial p}{\partial z}\right)=6\omega\frac{\partial}{\partial x}(ph) \tag{1}$$

The following dimensionless parameters are defined:

$$\bar{x}=\frac{x}{0.5L},\bar{z}=\frac{z}{0.5L},\bar{p}=\frac{p}{p_0},\bar{h}=\frac{h}{0.002R} \tag{2}$$

Substituting Eq. (2) into Reynolds Eq. (1), the dimensionless form of the Reynolds equation is given by:

$$\frac{\partial}{\partial \bar{x}}\left(\bar{h}^3\frac{\partial \bar{p}^2}{\partial \bar{x}}\right)+\frac{\partial}{\partial \bar{z}}\left(\bar{h}^3\frac{\partial \bar{p}^2}{\partial \bar{z}}\right)=\Lambda_x\frac{\partial}{\partial \bar{x}}(\bar{p}\bar{h}) \tag{3}$$

where

$$\Lambda_x=\frac{6R\omega\eta L}{p_a(0.002R)^2}$$

The film thickness (h) for the foil bearing is

$$h=C+e\cos(\theta-\varphi)+w_d \tag{4}$$

where C and e are the radial clearance and journal eccentricity, φ is the attitude angle. w_d is the deflection of the support structure.

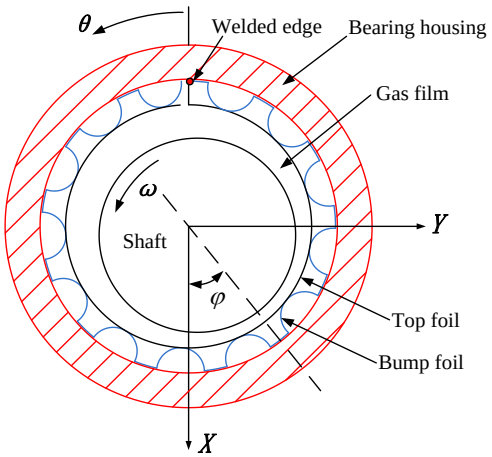

Figure 1 Structure of first generation bump foil bearing

Simple elastic foundation model [5, 6]

Heshmat used Wallowit's bump static stiffness equation to analyze gas foil bearing by proposing some assumptions:

(1) The stiffness of the bump foil is taken to be uniformly distributed and constant throughout the bearing surface. The stiffness of single bump K_B is constant and independent of bump deflection.
(2) The top foil is not deflect relative to the bumps but follows the deflection of the bumps themselves.

So the support structure deflection w_d can be written as:

$$w_d=\frac{\delta p_A}{K_B s} \tag{5}$$

where $\delta P_A=1/L\int_0^L(p-p_a)\,dz$, $K_B=\frac{E_B t_B^{\,3}}{2(1-\nu_b^{\,2})l^3}$, p_a is the ambient pressure beneath the foil and s is the single bump pitch.

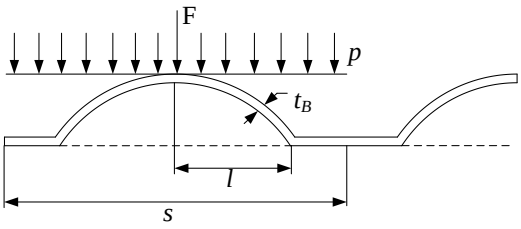

Figure 2 Configuration of bump foil [5, 6]

1-D analytical beam model [14]

Kim used the simple 1-D analytical beam model for top foil deflection by proposing some assumptions:

(1) The top foil is divided into multiple foil strips of the same number as the computational grid points along the axial direction in order to consider the axial variation of the top deflection.

(2) The axial deflection of each foil strip is dependent of the others.

Fig. 3 depicts the computational scheme of 1-D analytical beam model for top foil deflection. Where $p_{2Bi-1,j}$, $p_{2Bi,j}$ and $p_{2Bi+1,j}$ are the nodal pressures force on top foil, $k_{Bi,j}$ and $k_{Bi+1,j}$ are the stiffness of two adjacent bumps.

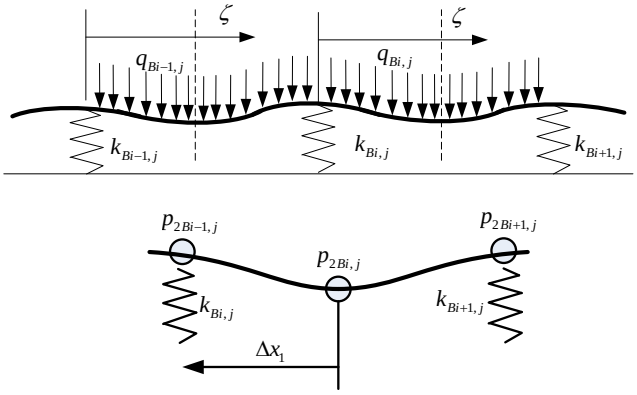

Figure 3 1-D analytical beam model for top foil deflection [14]

Each top foil segment ($\zeta = 0 - 2\Delta x_1$) is modeled as a slender beam with ends clamped at both sides but free to move along the horizontal direction. In order to obtain the top foil local deflection $v_{Bi,j}(\zeta)$, both bump supports are assumed to be rigid, so the $v_{Bi,j}(\zeta)$ can be solved using the following equation with zero deflections and slopes at both ends:

$$\begin{aligned} EIv''''_{Bi,j} &= q_{Bi,j}(\zeta) \\ v_{Bi,j}(0) &= v_{Bi,j}(2\Delta x_1) = 0 \\ v'_{Bi,j}(0) &= v'_{Bi,j}(2\Delta x_1) = 0 \end{aligned} \tag{6}$$

where EI is the bending stiffness of the top foil segment. $q_{Bi,j}(\zeta)$ is the unit load distribution on each top foil segment between two adjacent bumps with index $B_{i,j}$ and $B_{i+1,j}$, and it follows a parabolic function:

$$q_{Bi,j}(\zeta) = (a_{Bi,j}\zeta^2 + b_{Bi,j}\zeta + c_{Bi,j})\Delta z \tag{7}$$

where coefficients $a_{Bi,j}$, $b_{Bi,j}$, and $c_{Bi,j}$ are to be decided by pressures on the top foil, and z is the axial coordinate of the bearing.

The coefficient $a_{Bi,j}$, $b_{Bi,j}$, and $c_{Bi,j}$ turn out to be

$$\begin{aligned} a_{Bi,j} &= \frac{p_{2Bi+1,j} - 2p_{2Bi,j} + p_{2Bi-1,j}}{2\Delta x_1^2} \\ b_{Bi,j} &= \frac{4p_{2Bi,j} - 2p_{2Bi+1,j} + 3p_{2Bi-1,j}}{2\Delta x_1} \\ c_{Bi,j} &= p_{2Bi-1,j} \end{aligned} \tag{8}$$

where Δx_1 corresponds to the distance between computational grid points along the circumferential direction.

The bump deflection under the parabolic load distribution given by Eq. (7) can be calculated from the following bump dynamic equation, neglecting the inertia of the top and bump foils:

$$f_{Bi,j} = k_{Bi,j}\delta_{Bi,j} + c_{Bi,j}\dot{\delta}_{Bi,j} \tag{9}$$

where $k_{Bi,j}$ and $c_{Bi,j}$ are the stiffness and equivalent viscous damping coefficients of the bumps, respectively. The equivalent viscous damping coefficient can be given by $c_{Bi,j} = \gamma k_{Bi,j}/\omega$ through the structural loss factor γ if the bump motion is assumed as sinusoidal during normal imbalance excitations. The force, $f_{Bi,j}$ on a bump *Bi,j* can be calculated by integration of Eq.(7) over the region between the lower and upper limits in Fig. 3.

$$\begin{aligned} f_{Bi,j} &= \left(\int_{\Delta x_1}^{2\Delta x_1} q_{Bi,j}(\zeta)\mathrm{d}\zeta + \int_0^{\Delta x_1} q_{Bi,j}(\zeta)\mathrm{d}\zeta\right)\Delta z \\ &= \frac{1}{12}(-p_{2Bi-2,j} + 13p_{2Bi-1,j} + 13p_{2Bi,j} - p_{2Bi+1,j})\Delta x_1 \Delta z \\ &= \bar{p}_{Bi,j}\Delta x_1 \Delta z \end{aligned} \tag{10}$$

Once the bump deflection $\delta_{Bi,j}$ is calculated, the top foil deflection at ζ can be calculated by adding the top foil local deflection to the bump deflection

$$\begin{aligned} w_{Bi,j}(0) &= \delta_{Bi,j} \\ w_{Bi,j}(2\Delta x_1) &= \delta_{Bi+1,j} \\ w_{Bi,j}(\zeta) &= \left(1 - \frac{\zeta}{2\Delta x_1}\right)\delta_{Bi,j} + \frac{\zeta}{2\Delta x_1}\delta_{Bi+1,j} + v_{Bi,j}(\zeta) \end{aligned} \tag{11}$$

Beam model for top foil [13, 17]

For convenience, the top foil is usually modeled as 1-D Euler-beam in some literatures and the finite element stiffness matrix of Euler beam k_e is:

$$\mathrm{k_e} = \frac{EI_z}{L_b^3}\begin{bmatrix} 12 & 6L_b & -12 & 6L_b \\ 6L_b & 4L_b^2 & -6L_b & 2L_b^2 \\ -12 & -6L_b & 12 & -6L_b \\ 6L_b & 2L_b^2 & -6L_b & 4L_b^2 \end{bmatrix} \tag{12}$$

where *E* is the plate elastic modulus, the I_z and L_b are the area

moment of inertia about z axis and the length of beam. But actually, the top foil in the bearing house is curved. So in this paper, the 1-D curved beam model is given to compare with other top foil models.

Fig. 4 depicts the one dimensional model of the top foil. One end of the top foil is fixed with the transverse deflection and rotation equal to zero, while the other end is free. The bump strip layer beneath the top foil is in the same situation. The freedom degrees of 1-D model are shown as transverse deflections (w_d) and rotations (ϕ_z).

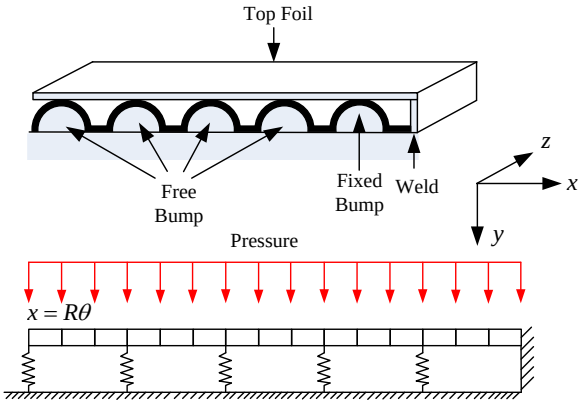

Figure 4 1-D structure model for bump foil bearing [13]

The curved beam model is shown in Fig. 5. x_c, y_c, z_c are the natural (local) curved element coordinates, $\bar{x}_c, \bar{y}_c, \bar{z}_c$ are the generalized element coordinates, and X_c, Y_c, Z_c are the global coordinates. For thin beams without shear deformation effects and rotary inertia, the radius of neutral axis of bar r_n is equal to radius of centroidal line of bar R_c. Pilkey [17] details the elasticity equations for deformation in a thin curved beam. For the beam model, the finite element method is used to obtain the transverse deflections (w_d). Curved beam element stiffness matrix k^i in the natural (local) curved element coordinate system is:

$$\tilde{\mathrm{k}}^i = \mathrm{QS} \tag{13}$$

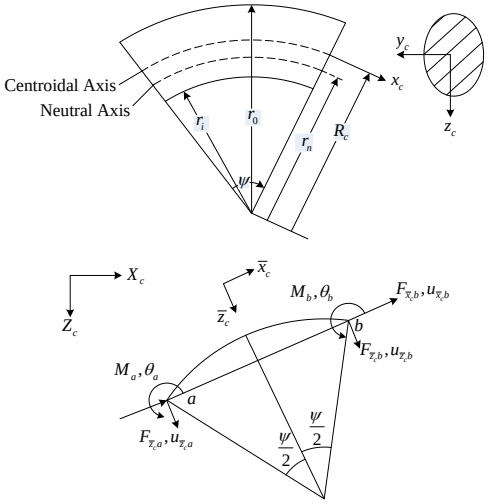

Figure 5 Curved beam element [17]

where **Q** and **S** are the coefficient matrices for curved beam element and detailed in ANNEX A. The 6×6 element stiffness matrices k^i in the global coordinate system are obtained using:

$$\mathrm{k}^i = \mathrm{T}^{i\mathrm{T}}\,\mathrm{k}^i\,\mathrm{T}^i \tag{14}$$

where T^i is the transformation matrix for in-plane loading stiffness matrices and can be written as:

$$\mathrm{T}^i = \begin{bmatrix} \cos\bar{x}_c X_c & \cos\bar{z}_c X_c & 0 & 0 & 0 & 0 \\ \cos\bar{z}_c X_c & \cos\bar{z}_c Z_c & 0 & 0 & 0 & 0 \\ 0 & 0 & 1 & 0 & 0 & 0 \\ 0 & 0 & 0 & \cos\bar{x}_c X_c & \cos\bar{z}_c X_c & 0 \\ 0 & 0 & 0 & \cos\bar{z}_c X_c & \cos\bar{z}_c Z_c & 0 \\ 0 & 0 & 0 & 0 & 0 & 1 \end{bmatrix} \tag{15}$$

where $\bar{x}_c X_c$ is the angle between $\bar{x}_c$ and X_c; and so on, for $\bar{z}_c X_c$, $\bar{z}_c Z_c$. For the curved beam element model is one dimensional, the transformation matrix T^i is an identity matrix and the model deflections in x direction in Fig. 4 are not considered.

The top foil model stiffness matrix [$\mathbf{K^T}$] in the global coordinate system can be obtained by adding the curved beam element stiffness matrices one by one. Meanwhile, the bump foil stiffness matrix in the global coordinate system [$\mathbf{K^B}$] is derived from the single bump stiffness using Iordanoff's equation, K_{FF} and K_{FW} are the stiffness for a free-free ends bump and a fixed-free end bump respectively. The global stiffness matrix of total model [$\mathbf{K^G}$] shown in Fig. 6 can be obtained through adding the bump foil stiffness matrix [$\mathbf{K^B}$] to the top foil model stiffness matrix [$\mathbf{K^T}$], m is the element number between two adjacent bumps, the express is written as follows:

$$[\mathbf{K^G}] = [\mathbf{K^T}] + [\mathbf{K^B}] \tag{16}$$

For the top foil fixed end is welded, $v = \phi_z = 0$ where v is the top foil deflection in y direction and ϕ_z is the rotation angle about z axis. The equation for deflections of total model in the global coordinate system is given by:

$$[\mathbf{K^G}]\,\{\mathbf{U^G}\} = \{\mathbf{F^G}\} \tag{17}$$

where $\{\mathbf{U^G}\}$ is the vector of displacement and $\{\mathbf{F^G}\}$ is the vector of pressures acting on the top foil. The expressions of $\{\mathbf{U^G}\}$ and $\{\mathbf{F^G}\}$ are written as follows:

$$\left\{\mathrm{U^G}\right\} = \left\{u_1 \quad v_1 \quad \phi_{z1} \quad u_2 \quad v_2 \quad \phi_{z2} \quad \cdots\cdots\right\}^T \tag{18}$$

$$\left\{\mathrm{F^G}\right\} = \left\{0 \quad p_1 \quad 0 \quad 0 \quad p_2 \quad 0 \quad \cdots\cdots\right\}^T \tag{19}$$

where u_1, u_2 … are the deflections of the top foil in x direction which are not considered in analysis process, p_1, p_2 … are the pressures acting on the top foil element nodes.

The finite element analysis is taken before solving the thin gas film governed by Reynolds Eq. (3) and its results w_d is used for Eq. (4) to update the film thickness.

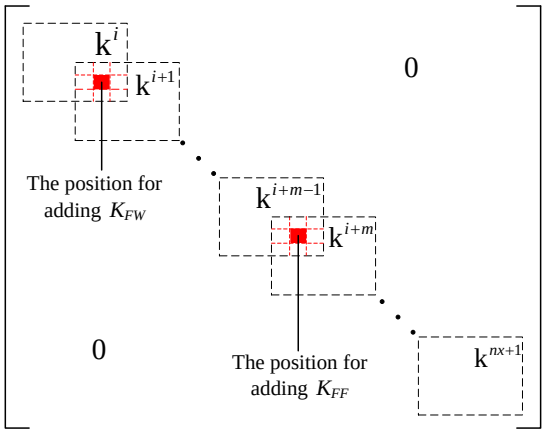

Figure 6 Stiffness matrix [K^G]

Solution with Newton-Raphson method

Newton-Raphson iteration of function $F(\bar{p})$ is written as follows:

$$F\left(\bar{p}^n\right)+F'\left(\bar{p}^n\right)\delta=0 \tag{20}$$

where

$$\delta=\bar{p}^{n+1}-\bar{p}^n,\quad n=0,1,2,\cdots,$$

Expanding function $F\left(\bar{p}+\beta\delta\right)$ in the form of a Taylor series about $\bar{p}$, and do the first derivative with respect to β, the approximate expression form is obtained:

$$\frac{dF\left(\bar{p}+\beta\delta\right)}{d\beta}\Big|_{\beta=0}=\delta F'\left(\bar{p}\right)=-F\left(\bar{p}\right) \tag{21}$$

RESULTS AND DISCUSSION

Method validating

The purpose for this part is to verify the results of the proposed method by comparing with the numerical predictions reported in Ref. [9]. The simulated bearing is a first generation foil bearing and its data is shown in Table 1.

According to Ref. [9], comparison of steady-state film thickness of bearing under the action of the corresponding hydrodynamic pressure is shown between foil bearing and rigid bearing in certain condition. In Fig. 8, the numeric results using the method mentioned in this paper are compared with predictions of gas foil bearing in Ref. [9]. The pressure distribution and film thickness are almost the same.

Table 1. Bearing data. Ref. [9]

Shaft radius (R)	50×10^{-3} m
Bearing length (L)	75×10^{-3} m
Radial clearance (C)	100×10^{-6} m
Top foil thickness (t_T)	101.6×10^{-6} m
Bump foil thickness (t_B)	76.2×10^{-6} m
Bump foil Young's modulus (E_B)	207×10^{-9} N/m^2
Bump foil Poisson's ratio (ν_b)	0.3
Bump friction coefficient (f)	0
Bump length ($2l$)	3.434×10^{-3} m
Bump pitch (s)	4.064×10^{-3} m
Bump height (h_B)	0.63×10^{-3} m
Air viscosity (η)	1.932×10^{-5} Pa•s
Air density (ρ_0)	1.1614 Kg/ m^3
Atmospheric pressure (p_a)	1.01325×10^{-5} Pa

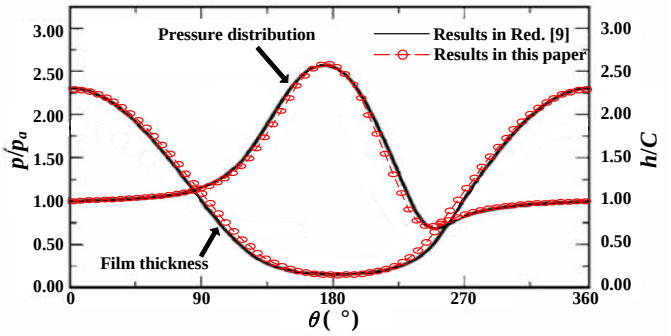

Figure 7 Comparison of pressure distribution and corresponding film thickness of a foil bearing with numerical results in [9] (ω = 30 krpm, h_{min} = 16μm)

Hydrodynamic performance

The analysis results of foil bearing models are compared with experimental data in literature to verify its validity. The parameters for the test first generation foil bearing in Ref. [19] are summarized in Table 2. The top foil and bump foil are spot welded together at one end to the bearing house. The other ends of top foil and bump foil are both free. The bump foil stiffness per unit area (K_f) is given by Iordanoff's equation [10, 18]: K_{ff} = 4.7×10^9N/m^3, K_{fw} = 10.4×10^9N/m^3 for a free-free ends bump and a fixed-free end bump respectively.

Table 2. Bearing data. Ref. [19]

Shaft radius (R)	19.05 mm
Bearing length (L)	38.1 mm
Radial clearance (C)	31.8 μm
Top foil thickness (t_T)	101.6 μm
Bump foil thickness (t_B)	101.6 μm
Bump foil Young's modulus (E_B)	214 GPa
Bump foil Poisson's ratio (ν_b)	0.29
Half bump length (l)	1.778 m
Bump pitch (s)	4.572 mm
Bump height (h_B)	0.508 mm
Foil arc circumferential length (l_x)	120 mm
Number of bumps (N_B)	26

The gas foil bearing simulation using the simple elastic foundation model, 1-D analytical beam model, 1-D Euler-beam model and 1-D curved beam model, predict the static performance of the test bearing. As the first generation bump foil bearing structure is symmetrical about the mid-plane, the results are presented for only half of the bearing. All of the models use a mesh of 78 and 10 elements in the circumferential and axial direction. So the bump stiffness for a free-free ends bump and a fixed–free end bump are:

$$K_{FF} = K_{ff} \times A_b = 40935.4 \text{ N/m}$$

$$K_{FW} = K_{fw} \times A_b = 90580.5 \text{ N/m}$$

Here the elastic modulus for the top foil is artificially increased, $E_T = E_B \times S_{fc}$, where S_{fc} is a stiffening factor along the circumferential direction, E_B and E_T are the elastic modulus for the bump foil and top foil, respectively. In Ref. [13], $S_{fc} = 4$, so the modulus of top foil is $E_T = 856$ GPa.

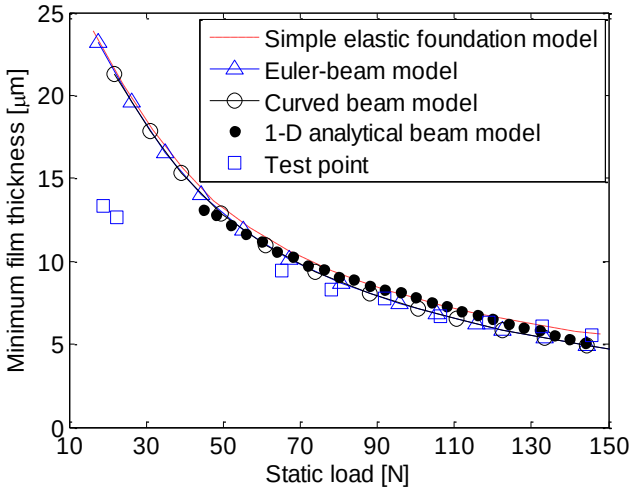

(a) 30,000 rpm

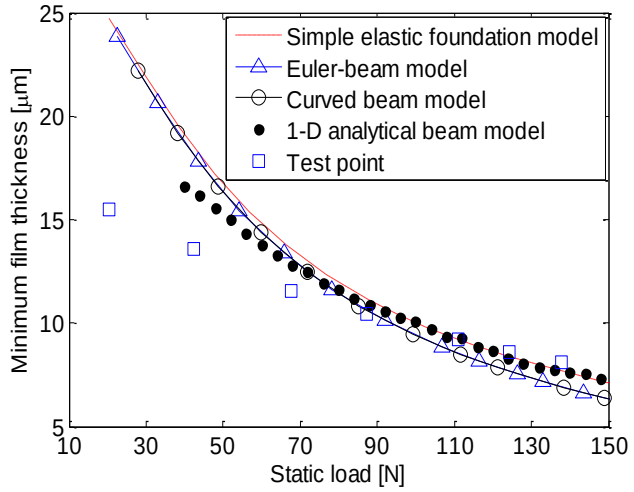

(b) 45,000 rpm

Figure 8 Minimum film thickness at mid-plane versus static load for four foil structure models and test data [19] at two shaft speeds

Fig. 8 presents the minimum film thickness versus static load for operation at shaft speed (a) 30,000 rpm and (b) 45,000 rpm, respectively. The figure is comprised of predictions for four foil bearing models and the test data. The simulation and test data are both at the bearing mid-plane. For the same static load, the 1-D curved beam model prediction is almost the same as 1-D Euler-beam model prediction. However they are both smaller than simple elastic foundation model, especially on the heavy static load condition. The 1-D analytical beam model predictions agree best with the test data.

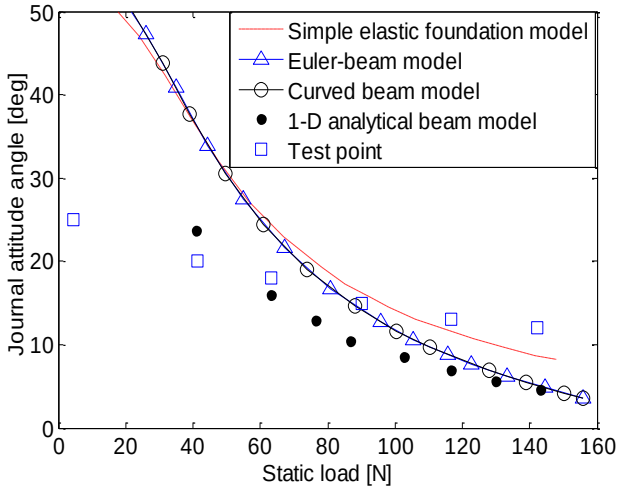

(a) 30,000 rpm

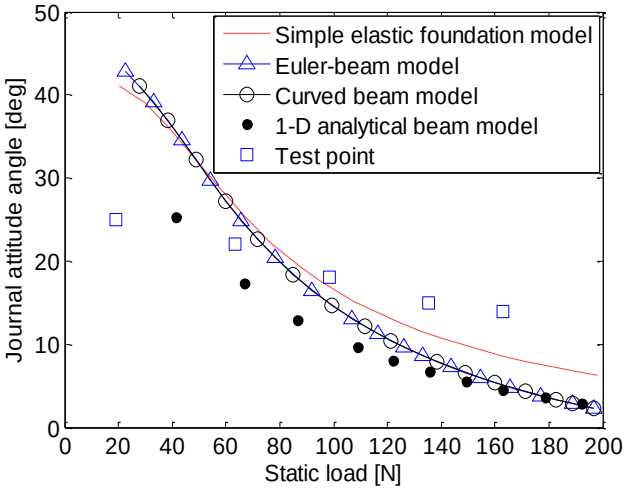

(b) 45,000 rpm

Figure 9 Journal attitude angle versus static load for four foil structure models and test data [19] at two shaft speeds

Fig. 9 shows the journal attitude angle versus static load at shaft speed (a) 30,000 rpm and (b) 45,000 rpm. The figure includes predictions for four foil bearing models and the test data [19]. Predictions of simple elastic foundation model, 1-D Euler-beam model and 1-D curved beam model overestimate the test data below 80 N while underestimate the test data above 80 N. These simulation results are different from numerical predictions in Ref. [13]. As the speed increase, predictions of all models above 80 N underestimate the test data increasingly, while it is just the contrary below 80 N. when static load is small, the discrepancy between 1-D analytical beam model predictions and the test data is small, but it becomes bigger with the increasing of static load.

The predicted dimensionless pressure distribution (p/p_a) and the top foil deflection for 1-D curved beam model are depicted in Fig. 10 and Fig. 11, respectively. The static load is 134.1 N and the shaft speed is 30,000 rpm. The dimensionless pressure is smaller than 1($p<p_a$) and pressure decreases

dramatically from mid-plane to bearing edge. The top foil deflection values are corresponding to the dimensionless pressure along circumferential location. If the dimensionless pressure is smaller than 1, the foil deflection value can be negative.

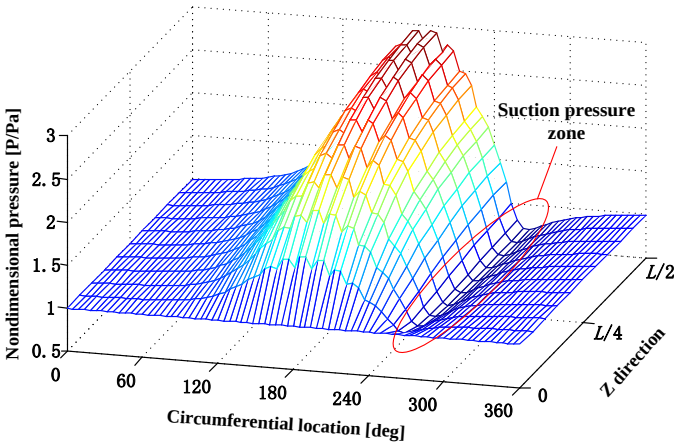

Figure 10 Predicted dimensionless pressure distribution for 1-D curved beam model. Static load: 134.1 N, shaft speed: 30 krpm

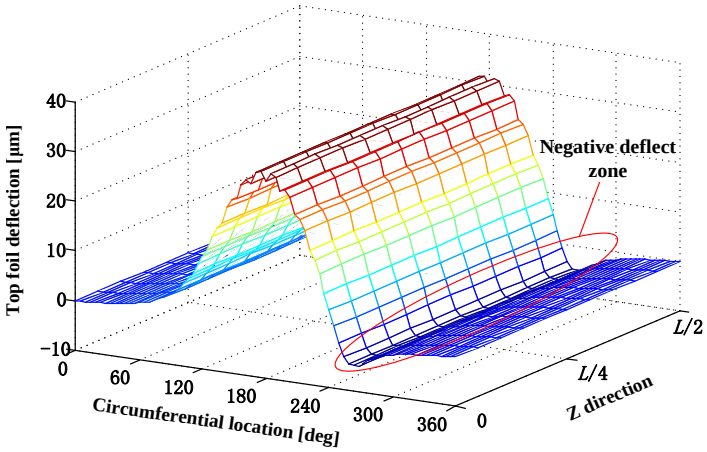

Figure 11 Predicted top foil deflection for 1-D curved beam model. Static load: 134.1 N, shaft speed: 30 krpm

The maximum top foil deflection is about 31.8μm and it is 1.67 ‰ of the top foil radius. In this magnitude, curvature effects of beam model can be ignored. This is the reason for the predictions of 1-D Euler-beam model and 1D curved beam are similar.

At the same operation condition, the predicted film thickness versus circumferential location for 1-D curved beam model and measured film thickness [19] are shown in Fig. 12. At the smallest film thickness zone, there exists sagging phenomenon for the prediction and the measurement. It is due to the softness of top foil in adjacent two bumps. The smallest film thickness zone for prediction is a little larger than test data, but at most smallest film thickness zone the two curves correlate well.

Note that: the 1-D curved top foil structural model has the biggest computational costs than the other models due to its element stiffness matrix dimension.

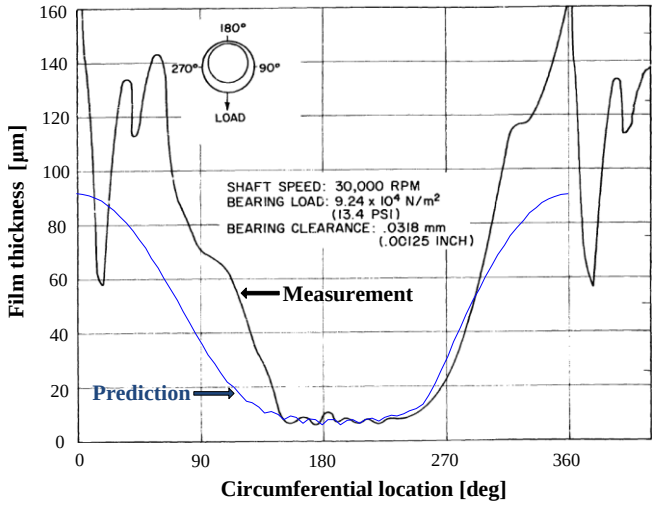

Figure 12 Predictions of film thickness for 1-D curved beam model and test data [19] at bearing mid-plane. Static load: 134.1 N, shaft speed: 30 krpm

The results presented here for the half bearing were calculated using a uniform mesh with 78 elements in the circumferential direction and 10 elements in the bearing length direction. The comparison of the results with 78 by 10 elements and 156 by 20 elements shown in Fig. 13 demonstrates that the results are independent of mesh density.

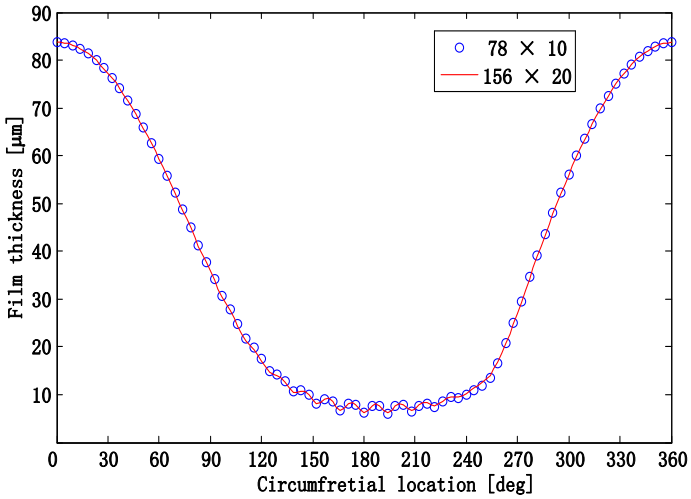

Figure 13 Comparison of gas film thickness for 1-D curved beam model at bearing mid-plane with different mesh density. Eccentricity: 52 μm, shaft speed: 30 krpm

CONCLUSIONS

A hydrodynamic analysis of a specific foil bearing is done to verify the accuracy of the Newton-Raphson method and finite difference method. The compressibility of the lubricant and the bearing compliance are both considered. Numerical results such

as pressure distribution and film thickness agree well with the numerical results applied from literature.

On the basis of above work, specific gas foil bearing is analyzed and compared with existing experimental data. 1-D Euler-beam model and 1-D curved beam model are developed and analyzed using finite different method coupled with finite element method. Predictions of gas foil bearing minimum film thickness for increasing static loads and two shaft speeds agree well with the test data, especially at low shaft speed. Predictions of two beam models are almost the same and both underestimate the film thickness. Minimum film thickness predictions of 1-D analytical beam model are the closest to experimental results. Comparison of gas foil bearing attitude angle predictions between foil bearing models and test data is taken for increasing static loads and two shaft speeds. Predictions of all models (except 1-D analytical beam model) overestimate the test data above 80 N while underestimate the test data below 80 N. In addition, the predicted dimensionless pressure distribution (p/p_a) and the top foil deflection for 1-D curved beam model under certain condition are presented. The predicted film thickness versus circumferential location for 1-D curved beam model is similar to experimental measurement at the smallest film thickness zone. The sagging phenomenon of the top foil can be seen due to the softness of top foil in adjacent two bumps. But as the measurements of film thickness had an uncertainty of 15% reported in [19], it is hard to make sure which model is the best. The present work in this paper is the preparation for future research of 2-D curved beam model which the stretch effect in circumferential direction is considered.

REFERENCES

[1] Agrawal, G. L., 1997, "Foil Air/Gas Bearing Technology - an Overview," ASME Paper No. 97-GT-347.Put references here.

[2] Feng, Kai., Kaneko, Shigehiko., 2010, "Analytical Model of Bump-Type Foil Bearings Using a Link-Spring Structure and a Finite-Element Shell Model," ASME Journal of Tribology, 132, pp. (021706) 1-11.

[3] Blok, H., van Rossum, J. J., 1953, "The Foil Bearing-A New Departure in Hydrodynamic Lubrication," Lubrication Engineering, Vol.9, No.6, Dec., pp. 316-320.

[4] Walowit, J. A., Anno, J. N., 1975, Modern Developments in Lubrication Mechanics, Applied Science Publishers Ltd, London, UK, Chap. 7.

[5] Heshmat, H., Walowit, J. A., Pinkus, O., 1983, "Analysis of Gas-Lubricated Foil Journal Bearings," ASME Journal of Lubrication Technology, 105, pp. 647-655.

[6] Heshmat, H., Walowit, J. A., Pinkus, O., 1983, "Analysis of Gas-Lubricated Complaint Thrust Bearings," Transactions of the ASME, 105, pp. 638-646.

[7] Peng, Z.-C., Khonsari, M. M., 2004, "Hydrodynamic Analysis of Compliant Foil Bearings With Compressible Air Flow," Transactions of the ASME, 126, pp. 542-546.

[8] Peng, Z.-C., Khonsari, M. M., 2004, "On the Limiting Load-Carrying Capacity of Foil Bearings," ASME Journal of Tribology, 126, pp. 817-818.

[9] Peng, Z.-C., Khonsari, M. M., 2006, "A Thermohydrodynamic Analysis of Foil Journal Bearings," Transactions of the ASME, 128, pp. 534-541.

[10] Iordanoff, I., 1999, "Analysis of an Aerodynamic Compliant Foil Thrust Bearing: Method for a Rapid Design," ASME Journal of Tribology, 121, pp. 816-822.

[11] Lez, Le, Sébastien., Arghir, Mihaï, Frene, Jean., 2007, "A New Bump-Type Foil Bearing Structure Analytical Model," ASME Journal of Engineering for Gas Turbines and Power, 129, pp. 1047-1057.

[12] Lee, D.-H., Kim, Y.-C., Kim, K.-W., 2004, "The Static and Dynamic Performance Analyses of Air Foil Journal Bearings for Various Bump Foil Stiffness," J. KSTLE, 20(5), pp. 245-251.

[13] San Andrés, L., Kim, T. H., 2007, "Improvements to the Analysis of Gas Foil Bearings Integrating of Top Foil 1D and 2D Structural Models," ASME Paper No. GT2007-27249.

[14] Kim, Daejong., Soongook, Park., 2009, "Hydrostatic Air Foil Bearings: Analytical and Experimental Investigation," Tribology International, 42, 413-425.

[15] Kim, Daejong., Creary, Andron., Chang, S. S., Kim, J. H., 2009, "Mesoscale Foil Gas Bearings for Palm-Sized Turbomachinery: Design, Manufacturing, and Modeling," J. Eng. Gas Turbines Power, 131, pp. (042502).

[16] Kim, Daejong., Creary, Andron., 2008, "IGA-Fabricated Meso Scale Foil Gas Bearings for Palm-Sized Microturbomachinery," Proceedings of the STLE/ASME International Joint Tribology Conference, October 20-22, 2008, Miami, Florida, USA, IJTC2008-71237.

[17] Walter D. Pilkey., 2004, *Formulas for Stress, Strain, and Structural Matrices (2 edition)*, Wiley, Chapters 13, 16.

[18] Kim, T. H., San Andrés, L., 2005, "Heavily Loaded Gas Foil Bearings: a Model Anchored to Test Data," ASME Paper No. GT2005-68486, ASME J. Eng. Gas Turbines Power.

[19] Ruscitto, D., Mc Cormick, J., and Gray, S., 1978, "Hydrodynamic Air Lubricated Compliant Surface Bearing For An Automotive Gas Turbine Engine I-Journal Bearing Performance," NASA CR-135368.

ANNEX A

COEFFICIENT MATRICES FOR CURVED BEAM ELEMENT

The modified top foil model used curved beam element based on the Pilkey's work in Ref. (17). The coefficient matrices for curved beam element are:

$$Q = \begin{bmatrix} 0 & 0 & 0 & 0 & -C_5 & 0 \\ 0 & 0 & 0 & 0 & 0 & -C_5 \\ 0 & -C_1 & 0 & 0 & -C_4\cos\beta & C_4\sin\beta \\ 0 & 0 & 0 & 0 & C_5 & 0 \\ 0 & 0 & 0 & 0 & 0 & C_5 \\ 0 & C_1 & 0 & 0 & C_4\cos\beta & C_4\sin\beta \end{bmatrix} \quad \text{(A.1)}$$

$$S = \begin{bmatrix} 0 & S_{12} & S_{13} & 0 & S_{15} & S_{16} \\ S_{21} & 0 & S_{23} & S_{24} & 0 & S_{26} \\ 1/2 & S_{32} & S_{33} & 1/2 & S_{35} & S_{36} \\ S_{41} & -1/2 & S_{43} & S_{44} & -1/2 & S_{46} \\ S_{51} & 0 & S_{53} & S_{54} & 0 & S_{56} \\ 0 & S_{62} & S_{63} & 0 & S_{65} & S_{66} \end{bmatrix} \quad \text{(A.2)}$$

where

$C_1 = EI/R^2$; $C_2 = \dfrac{AR^2 - I}{-AR^2 - I}$

$C_3 = \dfrac{2AR^2}{AR^2 + I}$; $C_4 = \dfrac{2EIA}{AR^2 + I}$

$C_5 = \dfrac{2EIA}{AR^3 + RI}$;

$\Delta_1 = 2C_3\sin^2\beta - 2\beta(C_2 + C_3)\cos\beta\sin\beta - 2\beta^2$

$\Delta_2 = 2(C_2 + C_3)\cos\beta\sin\beta - 2\beta$

$S_{12} = -(C_3\cos\beta)/\Delta_2$

$S_{13} = S_{16} = -R(C_2\cos\beta\sin\beta - \beta)/\Delta_2$

$S_{15} = (C_3\cos\beta)/\Delta_2$; $S_{21} = -(C_3\sin\beta)/\Delta_2$

$S_{23} = R(C_2\cos\beta\sin\beta + \beta)/\Delta_1$

$S_{24} = (C_3\sin\beta)/\Delta_2$

$S_{26} = -R(C_2\cos\beta\sin\beta + \beta)/\Delta_1$ (A.3)

$S_{32} = -(C_2\sin^2\beta - C_3\cos^2\beta)/\Delta_2$

$S_{33} = S_{36} = R(C_2\sin\beta - \beta\cos\beta)/\Delta_2$

$S_{35} = -(C_3\cos^2\beta - C_2\sin^2\beta)/\Delta_2$

$S_{41} = [C_3\sin\beta(\beta\sin\beta + \cos\beta) - \beta C_2\cos^2\beta]/\Delta_1$

$S_{43} = -R[\beta C_2\cos\beta + \beta(\beta\sin\beta + \cos\beta)]/\Delta_1$

$S_{44} = -[C_3\sin\beta(\beta\sin\beta + \cos\beta) - \beta C_2\cos^2\beta]/\Delta_1$

$S_{46} = R[\beta C_2\cos\beta + \beta(\beta\sin\beta + \cos\beta)]/\Delta_1$

$S_{51} = \beta/\Delta_1$; $S_{53} = -R(\sin\beta - \beta\cos\beta)/\Delta_1$

$S_{54} = -\beta/\Delta_1$; $S_{56} = R(\sin\beta - \beta\cos\beta)/\Delta_1$

$S_{62} = 1/\Delta_2$; $S_{63} = S_{66} = -(R\sin\beta)/\Delta_2$

$S_{65} = -1/\Delta_2$

and

R = Radius of centroidal line of beam

E = Modulus of elasticity

A = Area of cross section

I = Moment of inertia about y_c axis

β = Half angle of curved beam